Results in Materials 25 (2025) 100663

Contents lists available at ScienceDirect

Results in Materials

journal homepage: www.sciencedirect.com/journal/results-in-materials

Hot deformation behaviour, constitutive equations and processing map of Cu-Zn-Al-Ni shape memory alloy

Kenneth Kanayo Alaneme [a,b,*], Sodiq Abiodun Kareem [a], Justus Uchenna Anaele [a], Michael Oluwatosin Bodunrin [c]

[a] *Materials Design and Structural Integrity Group, Department of Metallurgical and Materials Engineering, The Federal University of Technology Akure, P.M.B. 704, Ondo State, Nigeria*

[b] *Centre for Nanoengineering and Advanced Materials, School of Mining, Metallurgy and Chemical Engineering, Faculty of Engineering & the Built Environment, University of Johannesburg, South Africa*

[c] *School of Chemical and Metallurgical Engineering, And DST–NRF Centre of Excellence in Strong Materials, All University of the Witwatersrand, Private Bag 3, WITS, 2050, Johannesburg, South Africa*

A R T I C L E I N F O

Keywords:
Cu-Zn-Al-Ni SMA
Hot deformation behaviour
Microstructure
Dynamic recrystallization
Processing maps
Constitutive equations

A B S T R A C T

The hot workability and deformation behaviour of Cu-Zn-Al-Ni based shape memory alloy (SMA) was investigated. The alloy was isothermal compression tested at temperatures of 250–550 °*C*, strain rates of 0.1–5 s^{-1}, and a constant total strain of 0.5, using a thermomechanical Gleeble-3500 simulator. The results show that positive strain rate sensitivity characterized the plastic flow behaviour of the SMA. The hyperbolic-sine constitutive equation - determined activation energy for the hot deformation of Cu-Zn-Al-Ni SMA (154.34 kJ/mol) is about 24 % lower than the activation energy for self-diffusion of copper, and that of the stress exponent value (n) which was less than 5, both point to dynamic recrystallization to be the dominant dynamic softening mechanism. Furthermore, the processing map indicated that flow instability occurs in the low temperature and strain rate regions (250 - 350 °*C*, 0.1 – 5s^{-1}) with characteristic shear bands, dendritic structures, and micro-cracks in their microstructure. The temperature of 550 °*C* and strain rates of between 0.1 and 2.5 s^{-1}, was established to be the optimal condition for hot deformation of the alloy. These conditions result in stable flow with microstructures consisting of fine dynamically recrystallized grains.

1. Introduction

Shape Memory Alloys (SMAs) are a unique class of intelligent materials that exhibit the capacity to regain their original structure following significant strain in response to mechanical force - superelasticity (SE) or thermal effects - shape memory effect (SME) [1]. The thermomechanical responsive character of SMAs is on account of the martensitic transformation which they undergo at definite temperatures [2]. Owing to these unique properties, SMAs have been utilized in marine, civil and structural, aerospace, medical, sensing, robotic systems, automobiles, and industrial applications [3–5].

Ni-Ti SMA products dominate the SMA market at present but the Cu-based SMAs have been projected to grow at a faster rate of 8.3 % in terms of compound annual growth rate [6]. Many researchers have acknowledged the prominence of Cu-based SMAs and envisaged them to replace NiTi SMAs in many applications on account of their good combination of mechanical and electrical properties as well as their cost-effectiveness [7]. These Cu-based SMAs are amenable to conventional casting procedures and have been widely reported to exhibit a moderate strain recovery of approximately 5 % (3 % less than NiTiSMA), which is acceptable for a large pool of shape memory applications [8]. They also have superior thermal conductivity (83 W/m·K) and electrical resistivity properties (2.8 × 10^{-4} Ω/mm) compared to 28 W/(m·K) and 8.3 × 10^{-4} Ω/mm obtained for NiTi SMAs [9]. Consequently, Cu-based SMAs are now preferred for utilization in electrical and thermo-responsive industrial and high-temperature applications such as in thermal actuators and sensors [10].

These Cu-based SMAs have some processing and functional limitations that have undermined their potential and impaired the expansion of their practical utilization [11]. These limitations which harm

* Corresponding author. Materials Design and Structural Integrity Group, Department of Metallurgical and Materials Engineering, The Federal University of Technology Akure, P.M.B. 704, Ondo State, Nigeria.

E-mail address: kalanemek@yahoo.co.uk (K.K. Alaneme).

https://doi.org/10.1016/j.rinma.2025.100663
Received 18 March 2024; Received in revised form 12 August 2024; Accepted 13 January 2025
Available online 14 January 2025

thermomechanical responsiveness and service reliability are related to their coarse and ordered structures which make them susceptible to cracking during forming and processing [12]. Another major drawback of Cu-based SMAs is the deterioration of their functional properties (especially the shape memory effect) due to spontaneous time-dependent structural changes caused by the phenomena of martensite stabilization [11]. Efforts have been made to resolve these constraints through several approaches, including alloy design, thermo-mechanical processing, and heat treatment [13].

Hot deformation is very important in materials design as it serves as a valuable process of developing finished products from cast ingots [14]. In hot deformation processing, the process parameters (deformation temperature, strain rate, and strain) play a major role in achieving high-quality products in terms of microstructures and materials properties [15]. Studies have shown that microstructural evolution during hot deformation is largely dependent on factors such as work hardening rates, deformation mechanisms, dynamic softening phenomena, and the critical stress needed for dynamic recrystallization (DRX) [16]. There is currently, limited understanding of the hot deformation characteristics of SMAs, which is responsible for the limited commercial and industrial adoption of hot deformation processes for SMA product design [1,17]. To develop Cu-Zn-Al-Ni SMAs with a high-performance index, there is a need to understand their hot deformation behaviour, which is vital for establishing the best hot working conditions to achieve optimized microstructures for products developed using SMAs. Thus, the objective of this investigation is to study the hot deformation behaviour and workability of Cu-Zn-Al-Ni SMAs and predict the safe zone and parameters for optimal processing.

2. Experimental process

2.1. Alloy design and production

Samples of Cu-Zn-Al SMAs modified with nickel were produced using copper pellets (purity 99.9 wt%), zinc billets (purity 99.8 wt%), Aluminum granules (purity 99.8 wt%), and nickel powder (purity 99.2 wt%). By following charge calculations, the starting materials were weighed, charged in a crucible furnace, melted, and cast in pre-heated stainless-steel molds. After the casting process, the ingot was removed from the mold and the specimen for microstructural characterization and thermo-mechanical tests were produced by the machining process. The chemical analysis of the SMA produced is presented in Table 1.

2.2. Thermo-mechanical processing

Specimens having a dimension of $\varnothing 8 \times 12$ mm were used for the isothermal hot compression test conducted at temperatures of 250 °*C*, 350 °*C*, 450 °*C*, and 550 °*C*, strain rates of 0.1 s^{-1}, 1.0 s^{-1}, and 5.0 s^{-1}, to a final strain of 0.5, utilizing a Gleeble 3500 thermo–mechanical simulator. Before each test, the center of the specimen is wrapped with a chromel–alumel thermocouple and heated at 5 °*C*/s to the deformation temperatures, and soaked isothermally for 180 s to ensure thermal homogenization of the specimen. Graphite foil and nickel paste were applied between the specimens and anvil to reduce friction during the testing. The samples were deformed by single–hit uniaxial compression until the required total strain was attained. The results of deformed specimens recorded and analyzed were only for those with a barrelling coefficient of less than 1.1. To maintain their microstructures, the samples were crushed and air-cooled immediately after each hot compression test. The stress-strain data obtained during the hot compression test was correlated with dynamic materials modeling (DMM) and used for the development of the processing map.

Table 1
Composition of the alloy sample.

Raw materials	Cu	Zn	Al	Ni
Weight percentage	74.7	18.0	7.0	0.3

2.3. Microstructural analysis

The microstructural analysis of the hot deformed samples of Cu-18Zn-7Al-0.3Ni SMAs was assessed using the Leica DM5000 optical microscopy (OM). To prepare the post-deformed samples for microstructural examination, they were cut parallel to the axis of deformation. The cut samples were then mounted with polyfast glue and polished to a mirror surface finish, following metallographic procedures outlined in Anaele et al. [3] and Alaneme et al. [18]. The samples were then etched with a solution of 5 g ferric chloride, 10 ml HCl, and 95 ml ethanol for 20 s after polishing with alumina powder.

3. Results and discussion

3.1. Microstructural characterization of Cu-18Zn-7Al-0.3Ni SMAs

The optical images showing the microstructural characteristics of the post-hot deformation samples of Cu-18Zn-7Al-0.3Ni SMAs at the experimental temperatures and strain rates are presented in Fig. 1. The microstructures were observed to exhibit elongated grain morphology with grain orientation perpendicular to the axis of deformation. The microstructure in all samples is characterized by two phases with elongated grains which represents a typical deformation structure. These microstructural features are consistent with the results on hot deformation of a Cu-based SMA, reported by Yong et al. [19]. Fig. 1a shows the optical images of the Cu-18Zn-7Al-0.3Ni SMA, hot compressed at 350 °*C* using varied strain rates. The microstructure consists of grains having dendritic morphology which is quite different from the microstructures obtained at higher temperatures (450 °*C* and 550 °*C*). The optical images presented in Fig. 1b and c represent the microstructures at hot deformation temperatures of 450 °*C* and 550 °*C* respectively and they possess comparable microstructural features. However, the microstructures show varied grain sizes with greater fine structures observed with the increase in deformation temperature. The microstructure of the SMA deformed at 450 °*C* is characterized by elongated grains which suggest the prevalence of dynamic recovery (DRV) over dynamic recrystallization (DRX). The microstructure of the Cu-Zn-Al-Ni alloy samples at 550 °*C* shows that nearly full dynamic recrystallization occurs at **0.1 s^{-1} and 1 s^{-1}** strain rates. This was attributed to the ease of dislocation climb, atom diffusion, and sub-grain boundary migration at higher temperatures, which all favour DRX grain formation. In addition, at low strain rates, the deformation speed is low, resulting in sufficient time for boundary migration, which facilitates the formation of DRXed grains [20,21]. This suggests that the formation of dynamically recrystallized grains in Cu-Zn-Al-Ni SMAs is favoured at higher deformation temperatures and low strain rates.

3.2. Stress-strain behaviour of Cu-18Zn-7Al-0.3Ni SMAs

The plastic flow behaviour of the SMAs when hot deformed is analyzed using the flow stress which is dependent on the deformation temperature, strain rate, and total strain [14]. The true stress-strain flow curves of the Cu-18Zn-7Al-0.3Ni SMA subjected to hot deformation at different strain rates and deformation temperatures are presented in Fig. 2. The decrease of peak flow stress with the increase in deformation temperature, and decrease with strain rate, characterized the positive strain rate sensitivity exhibited by the SMA. It has been well established in the literature that lower strain rates and high deformation temperatures are favourable conditions for the formation of DRX grains by mechanisms of grain boundary migration, formation of sub-grains, dislocation glide and climb which result in a decrease of the flow stress [14,22]. At high strain rates and low temperatures, the alloy shows a positive strain rate sensitivity with the attendant increase in

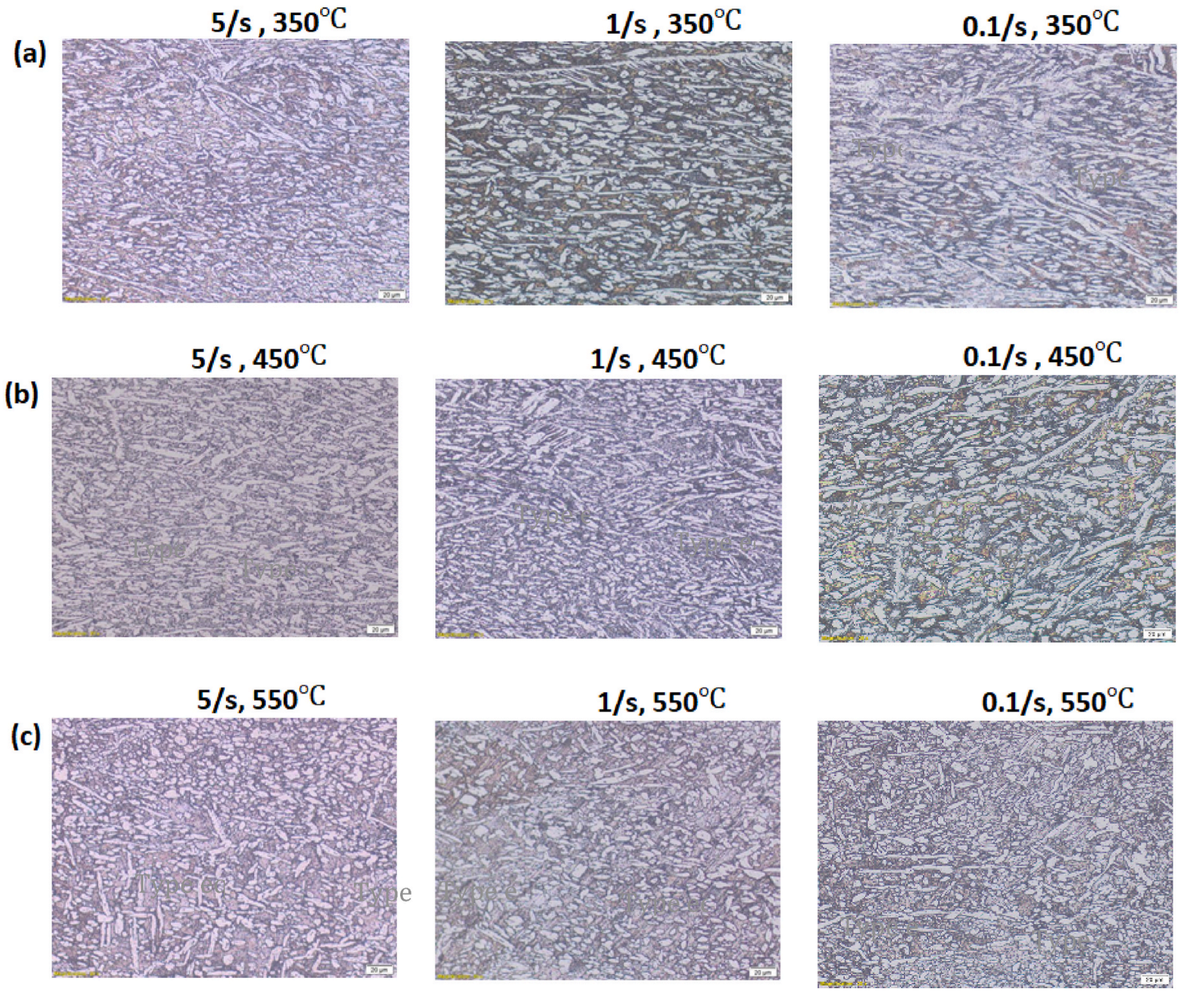

Fig. 1. Optical images showing the microstructural characteristics of the hot deformed samples of Cu-18Zn-7Al-0.3Ni SMAs at varied strain rates; (a) at 350 °C (b) 450 °C and (c) 550 °C

flow stress. This is attributed to the formation of heavy dislocation networks which renders dislocations immobile and impedes plastic flow by the mechanism of dislocation pinning action [19]. The stress-strain curves presented in Fig. 2a–c shows similar hot deformation trend with an initial rise in flow stress at low strains, attaining peak stress, and then show decline to a near constant flow stress value. The flow stress rapid rise at the onset of deformation is due to the proliferation of dislocation network leading to dislocation immobility, which results in the increase in the deformation stress [21]. Work hardening dominates the deformation mechanism at this stage, which persists until the attainment of peak stress. Sustained hot deformation with increasing strain and temperature, results in the tangled dislocations gaining kinetic energy, which facilitates dislocation annihilation by dislocation climb and gliding mechanisms, leading to the observed decline in the flow stress [19]. The flow stress decrease with increasing strain is attributed to the occurrence of dynamic recovery and recrystallization (DRV and DRX) which counterbalance the work hardening observed at the onset of deformation [23]. The nucleation and development of new grains that emerge from dynamic recrystallization is thought to be the mechanism responsible for the softening process [24]. The flow trend at the later deformation stage is characterized by steady-state flow stress, which normally arises due to the counter-balance between work hardening and dynamic softening rates [25]. Fig. 2d exhibits unique flow behaviour at relatively high deformation temperatures. An initial sharp increase was observed in the flow stress which was counterbalanced by the softening mechanism. The flow patterns exhibit swift hardening stage followed by an extensive softening and steady state flow regime suggesting the dominance of the softening mechanism over the strain hardening. The interaction between work hardening effect and softening mechanism leads to dynamic balance reached between the rate of work hardening and softening characterized by steady state flow at strain rate of $5s^{-1}$ and $1s^{-1}$. The Serrated flow behaviour observed in the flow curves (Fig. 2d) is ascribed to solute drag effect as a result of the tussle between the dislocation and solute atoms at elevated temperature thereby obstructing the dislocation motion. The optical microstructure of the sample deformed at 550 °C and $1s^{-1}$ strain rate revealed refined grains with a globular or nearly equiaxed shape, characteristics that align with the observed oscillations in the experimental flow curves. The results suggest that dynamic recrystallization and recovery of the samples are significantly influenced by the strain rates and deformation temperatures. This result is in accordance with the observations of Yong et al. [19], Santosh et al. [22], Zhang et al. [26], and Wang et al. [27] where it is explained that higher temperatures offer longer times for energy stockpile and higher interface migration which facilitates the nucleation DRX grains with an attendant decrease in the flow stress. In the quest to further elucidate the hot deformation characteristics of Cu-Zn-Al-Ni SMAs, prediction of the safe working zones and optimizing the hot deformation parameters for the alloy, were done using constitutive equations and processing maps, which are discussed in the succeeding sections of this paper.

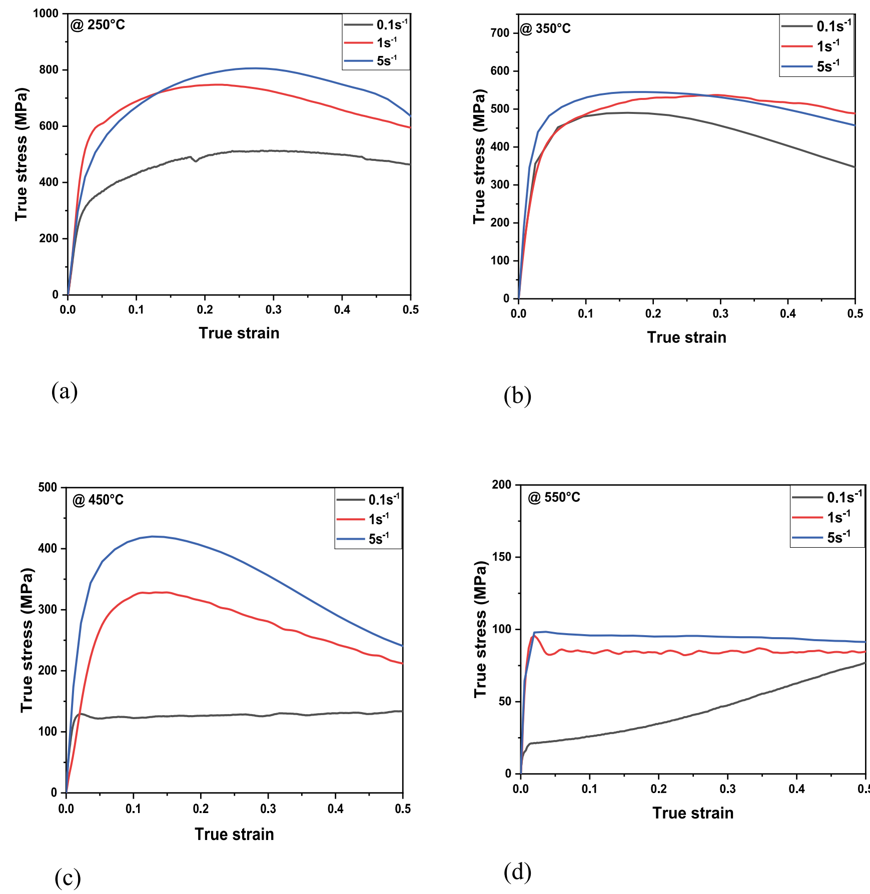

Fig. 2. Flow behaviour of Cu-18Zn-7Al-0.3Ni SMAs under hot compression at various strain rates and at (a) 250 °*C* (b) 350 °*C* (c) 450 °*C* (d) 550 °*C*

3.3. Constitutive equation

It is critical to examine the deformation characteristics of the Cu-Zn-Al-Ni SMA using constitutive equations to learn more about its hot deformation behaviour. The stress-strain curve data from hot compression experiments were utilized to predict the hot deformation behaviour of the alloy. Yong et al. [19], Zhang et al. [26], and Belbasi et al. [20] among others, have successfully used constitutive equations to predict the flow characteristics of hot deformation processed SMAs. In our study, the Arrhenius hyperbolic–sine constitutive equation (Eq. (1)) was used to predict the flow behaviour and determine the activation energy (Q) for hot deformation of Cu-Zn-Al-Ni SMA with respect to the Zener–Hollomon parameter (Z) which is a function of temperature and strain rate [28].

$$\dot{\varepsilon} = A\left[\sin h(\alpha\sigma p)^{n}\ \exp\left(\frac{-Q}{RT}\right) \text{for all}\ \sigma\right] \quad (1)$$

$$\sigma = \frac{1}{\alpha}\ln\left\{\left(\frac{Z}{A}\right)^{\frac{1}{n}} + \left[\left(\frac{Z}{A}\right)^{\frac{2}{n}} + 1\right]^{\frac{1}{2}}\right\} \quad (2)$$

where σ is the flow stress, Q is the activation energy for hot deformation, n is the stress exponent parameter, $\dot{\varepsilon}$ is the strain rate, R is the gas constant given as 8.314 kJ/mol, T is the temperature, Z is the Zener-Hollomon parameter, while α, β, and A represent the material constant. The stress sensitivity parameter is denoted by the constant n which is determined from (Eq. (1)) under conditions of lower stresses. The material constant α is known as the stress multiplier which is calculated from (Eq. (1)) and is related to the flow stress as follows: $\sigma = \frac{\beta}{\alpha}$; where σ is the peak stress derived from the stress-strain data, while β is calculated at peak stress using (Eq. (1)). The activation energy for the hot deformation process is determined from (Eq. (1)) following the plot log [sinh ($\alpha\sigma\rho$)] versus $1/T$. The model equation (Eq. (2)) is determined by fitting experimental data in the derivatives of the hyperbolic-sine data and by the input of the constitutive constants including α, n, β, and A [29]. The various graphs that illustrate how these constitutive constants were generated at the peak stress are presented in Fig. 3. The calculated values of the constitutive constants, activation energy, and peak flow stress are presented in Table 2. The constitutive model equation was validated and confirmed reliable by the computation of the correlation coefficient (R^2), and average absolute relative error (AARE) using Eqs. (3) and (4) [30].

$$\boldsymbol{AARE}\ (\%) = \frac{\mathbf{1}}{\boldsymbol{N}}\sum_{i=1}^{N}\left|\frac{\boldsymbol{M}_i - \boldsymbol{P}_i}{\boldsymbol{M}_i}\right| \times \mathbf{100} \quad (3)$$

$$\boldsymbol{R}^2 = \frac{\sum_{i=1}^{N}(\boldsymbol{M}_i - \overline{\boldsymbol{M}})(\boldsymbol{P}_i - \overline{\boldsymbol{P}})}{\sqrt{\sum_{i=1}^{N}(\boldsymbol{M}_i - \overline{\boldsymbol{M}})^2 \sum_{i=1}^{N}(\boldsymbol{P}_i - \overline{\boldsymbol{P}})^2}} \quad (4)$$

where $\boldsymbol{P}_i$ is the predicted stress, $\boldsymbol{M}_i$ is the measured stress, and $\boldsymbol{N}$ is the number of measurements [31].

There is a strong correlation between the measured stress and the predicted stress values, as indicated by the R^2 values (0.9295). The low value obtained for the average absolute relative error (0.6786) also suggests that the constitutive equation that was generated was very good at predicting flow stress during deformation. The accuracy and

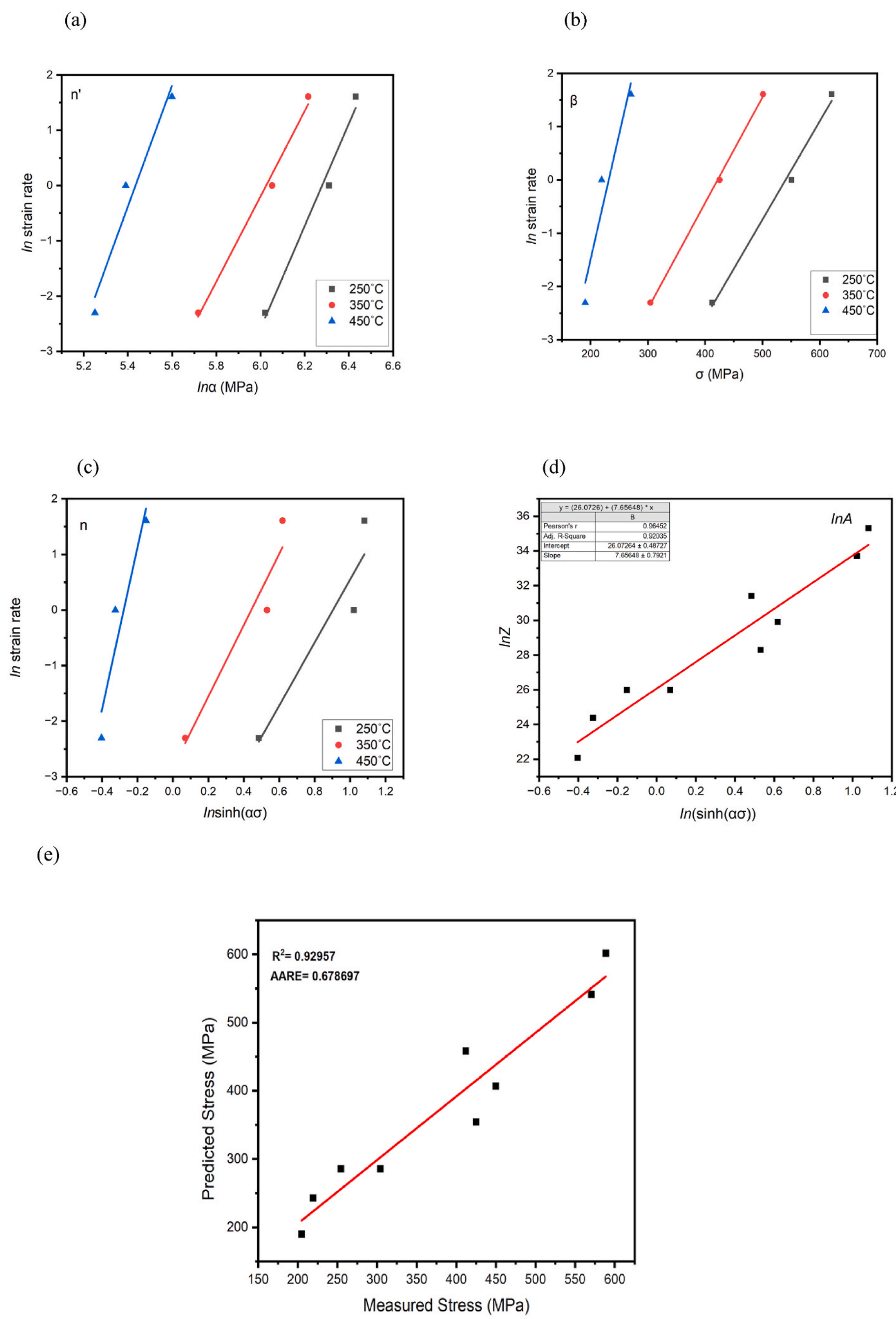

Fig. 3. Graphs illustrating the derivation of constitutive constants for Cu-Zn-Al-Ni SMA and showing the correlation of σ, $\dot{\varepsilon}$, T, and Z: (a) ln $\dot{\varepsilon}$ versus ln α (b) ln $\dot{\varepsilon}$ versus ln σ (c) ln $\dot{\varepsilon}$ versus ln[sinh($\alpha\sigma$)] (d) ln Z versus ln[sinh($\alpha\sigma$)] (e) Predicted stress (P_i) versus measured stress (M_i).

Table 2
Material constants for hot deformation of Cu-Zn-Al-Ni shape memory alloy.

α (MPa)	β	*ln* A	n	$\tilde{n}$	Q (kJ/Mol)	K
0.004407833	0.03335	32.796	4.540295119	7.566075	154.3428198	4.088766

dependability of the model have been shown to increase with a decreasing AARE value and R^2 value close to unity [32]. According to the statistical data, the obtained constitutive model equation was highly accurate and can correctly predict the deformation flow stress of the Cu-Zn-Al-Ni SMA. The results confirmed that DRX is the prevalent deformation mechanism since the activation energy for hot deformation (QHD) of the Cu-Zn-Al-Ni SMA is 154 kJ/mol which is 24.19 % less than the activation energy for self-diffusion (QSD) of copper-based alloys (203.6 kJ/mol). In FCC (face-centered cubic) alloys, the stacking fault energy (SFE) is significantly influenced by both the alloying elements and their concentrations [33]. In the case of copper alloys, the introduction of zinc and aluminium has been noted to induce planar slip, a departure from the wavy slip characteristic of pure copper [33]. This shift in behaviour is attributed to a reduction in stacking fault energy upon alloying with aluminium and zinc. In materials with low stacking fault energy, dynamic recrystallization is more thermodynamically viable and energetically feasible than dynamic recovery [19,33]. Studies have shown that dynamic recrystallization is active when the stress exponent (n) values are less than 5 [29,34]. It is thus deduced from Table 2 that the stress exponent of 4.54 obtained from the hot processing of Cu-Zn-Al-Ni SMA suggests that the DRX deformation mechanism is active. This result is consistent with the microstructures of the hot deformed SMA, which showed clear evidence of well-defined recrystallized grains. The employment of a hot processing map in the following section is necessary to establish the optimal hot deformation conditions for the processing of the Cu-Zn-Al-Ni SMA.

3.4. Theory of processing map

Nonlinear models are used to predict the flow behaviour during hot deformation processes by expressing the quantitative link between flow stress (σ) and temperature (T), strain rate ($\dot{\varepsilon}$), and strain (ε) [35]. Dynamic material models (DMM)–based processing maps have been successfully used for superalloys for microstructure prediction and deformation parameter optimization [36]. Both the power (G) expended during plastic deformation (called dissipator content) and the energy (J) dissipated from microstructural evolution which occur during the hot deformation process, contribute to the total power (P) dissipated during hot plastic deformation of SMAs [37]. Power dissipation (P) during hot deformation is calculated using DMM, which is founded on continuum mechanics and the irreversible thermodynamics of huge plastic flow [38,39]:

$$P = \sigma\varepsilon = G + J = \int_0^{\varepsilon} \sigma d\varepsilon + \int_0^{\sigma} \varepsilon d\sigma \tag{1}$$

where σ and ε are flow stress (MPa) and strain, respectively.

At constant T, σ and ε are related to $\dot{\varepsilon}$ by a power law relationship:

$$\sigma = K\dot{\varepsilon}^m \tag{2}$$

where m and K are the strain rate sensitivity and the material coefficient, respectively. The value of m can be expressed in terms of energy dissipated during hot deformation as follows:

$$m = \frac{\partial J}{\partial G} = \frac{\dot{\varepsilon}\partial\sigma}{\sigma\partial\dot{\varepsilon}} = \frac{\dot{\varepsilon}\sigma\partial\ln\sigma}{\sigma\dot{\varepsilon}\partial\ln\dot{\varepsilon}} \sim \frac{\Delta\log\sigma}{\Delta\log\dot{\varepsilon}} \tag{3}$$

At constant T and e, the dissipated co-content (J) is given as:

$$J = \int_0^{\sigma} \dot{\varepsilon}\partial\sigma = \frac{m\sigma\dot{\varepsilon}}{m+1} \tag{4}$$

Under the condition of ideal linear energy dissipation state where $m = 1$; J reaches maximum as J_{max} and given as:

$$J_{max} = \frac{\sigma\dot{\varepsilon}}{2} \tag{5}$$

The power dissipation efficiency (g) which is the ratio of J to J_{max} is expressed as:

$$\eta = \frac{J}{J_{max}} = \frac{2m}{m+1} \tag{6}$$

The power dissipation map is derived based on equation (6), which establishes a correlation between the power dissipation efficiency (g) and the processing parameters, T and $\dot{\varepsilon}$. Unstable flow observed during plastic deformation has been theoretically derived based on the maximum entropy principle. This principle yields an expression for the unstable flow of the material during plastic deformation [26]:

$$\xi(\dot{\varepsilon}) = \frac{\partial\left[\ln\frac{m}{m+1}\right]}{\partial\ln\dot{\varepsilon}} + m < 0 \tag{7}$$

The symbol $\xi(\varepsilon)$ represents the instability parameter, which is utilized for the instability map determination. The hot workability of metal alloys may be predicted by the analysis of the plastic flow instability curve [40]. The development of hot deformation processing maps requires the overlay of a power dissipation map and an instability parameter map, which is a plot depicting the logarithmic strain rate against deformation temperatures [41].

3.5. Processing map analysis

The establishment of the processing maps in terms of the power dissipation map and the instability parameter map is based on the stress-strain data presented in Table 1 as well as the flow curves given in Fig. 2. The results from these data showed that flow stress initially increase with strain before reaching a steady flow state due the competition between DRX and work hardening deformation mechanisms. Also, these results show a linear correlation between the logarithm of flow stress versus the strain rate which shows that Cu-Zn-Al-Ni SMA satisfies the condition for DMM of deformation.

It has been established that the relative rate of internal entropy created throughout the hot deformation is described by the power dissipation efficiency. The power dissipation maps for Cu-Zn-Al-Ni SMA at various strains are presented in Fig. 4. It is known from the literature that metal alloys with high η values are amenable to good hot workability during plastic deformation as the power input is effectively utilized by microstructural evolution via mechanisms of DRV, DRX and phase transformation. Conversely, lower η values suggest poor workability, and the microstructures are usually characterized by defects such as inhomogeneity and porosity [21,24]. It is observed from Fig. 4 that the region shaded red with temperature in the range of 500–550 $^\circ C$ and strain rates between 0.1 and 2.5 s^{-1} has $\eta > 30\%$ during the entire hot deformation process and represents the optimal hot deformation conditions for processing the Cu-Zn-Al-Ni SMAs. This is supported by the microstructure for the stable region or safe hot deformation zone for the Cu-Zn-Al-Ni SMAs at a deformation temperature of 550 $^\circ C$ and strain rate of 0.1 and $1s^{-1}$ presented in Fig. 5. The microstructure is characterized by uniform structures and fine equiaxed grains which signify the occurrence of dynamic recovery and recrystallization. Also, the region with blue shade observed in the low-temperature region (250–350 $^\circ C$) is characterized by low power dissipation efficiency in the range $17 \leq \eta \leq 29$ and is determined to be the unsafe zone for the hot deformation of the SMA. Unstable flow persists at all strain rates within this region at 250-350 $^\circ C$.

The photograph of the hot deformed samples shown in Fig. 6 supports the instability zones as the image is characterized by shear deformation and cracks at deformation temperature of 250 $^\circ C$. Fig. 7 shows the microstructure at 350 $^\circ C$ and strain rate of 0.1, 1, and $5s^{-1}$ characterized by structural inhomogeneity, dendritic structures, and micro-cracks in the deformed samples. On the other hand, the microstructure for the stable region or safe hot deformation zone for the Cu-Zn-Al-Ni SMAs at a deformation temperature of 550 $^\circ C$ and strain rate of 0.1 and $1s^{-1}$ is presented in Fig. 5. Hence, the power dissipation efficiency map shows high accuracy in predicting both the safe and unsafe processing parameters for this alloy.

The instability map of the Cu-Zn-Al-Ni SMAs is presented in Fig. 8. In literature, the zones exhibiting negative values for $\xi(\dot{\varepsilon})$ are classified as instability regions, wherein an unsteady flow of metals takes place during hot plastic deformation; whereas stable regions are defined as those with positive $\xi(\dot{\varepsilon})$ values, where stable metal flow occurs during hot plastic deformation [24]. It is observed from Fig. 8 that the instability map shows no instability region because the instability criteria $\xi(\dot{\varepsilon})$ has positive values. It therefore denotes that flow instability did not occur at peak stress in the deformed samples. This result agrees with the observations of some researchers including Jiang et al. [24], Santosh et al. [22], Zhang et al. [26], and Yong et al. [19]. The instability map

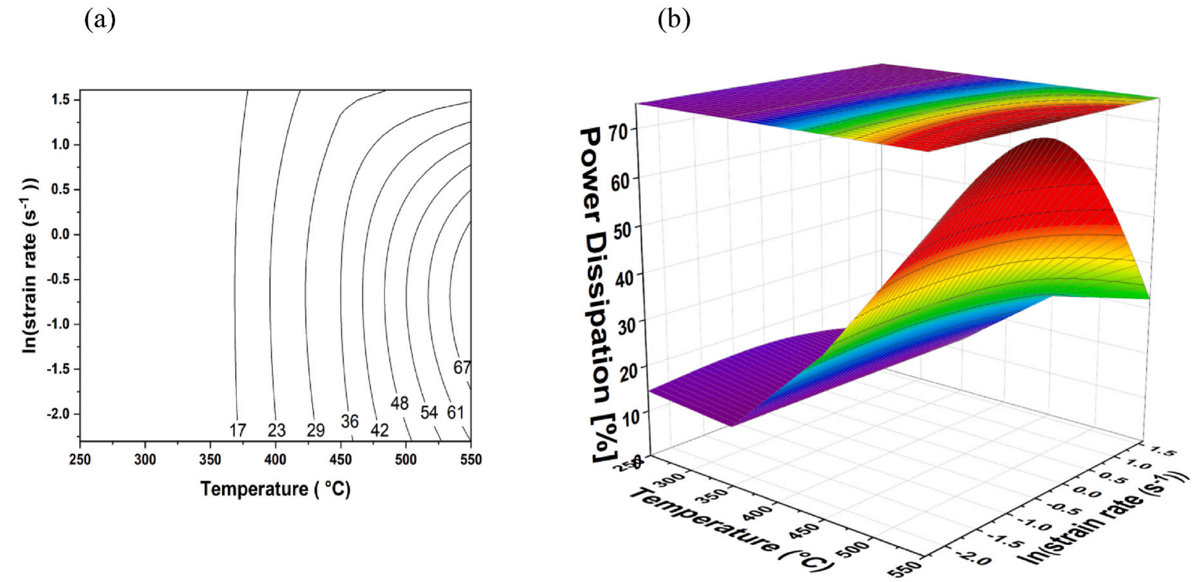

Fig. 4. Power dissipation map of Cu-Zn-Al-Ni SMA: (a) 2D power dissipation contour line map (b) 3D power dissipation surface map.

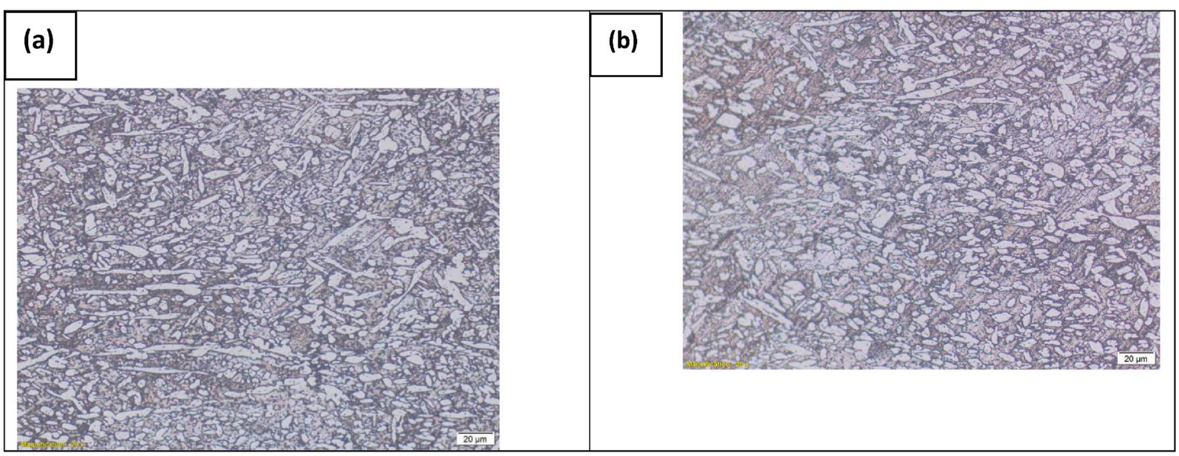

Fig. 5. Microstructures of Cu-Zn-Al-Ni SMA showing fine grain structures at 550 $^{\circ}C$ and strain rate of 0.1 and $1s^{-1}$.

Fig. 6. Photograph of the hot deformed samples at 250 $^{\circ}C$ showing shearing-type deformation.

showed that the optimum conditions for hot deformation of the Cu-Zn-Al-Ni SMAs exist at a temperature of 550 $^{\circ}C$ and 0.1–$2.5s^{-1}$ strain rates. Hence, the power dissipation efficiency map was used to establish the safe and unsafe processing parameters for this alloy.

The study suggests that DRV and DRX mechanisms characterizes the stable region and are responsible for obtaining high power dissipation efficiency during hot deformation of Cu-Zn-Al-Ni SMAs. It is known from the literature that high power dissipation efficiency signifies that a greater amount of power is utilized in phase transformation, DRV, and DRX processes which ultimately results in better hot workability of the material during hot deformation [24]. Therefore, the optimum parameters for the hot deformation of the SMA are in the region where $\eta\rangle$ 36% power efficiency, temperature of 550 $^{\circ}C$, and strain rates between 0.1 and $2.5s^{-1}$.

4. Conclusion

The hot deformation behaviour of Cu-Zn-Al-Ni SMA was investigated using hot compression testing conducted with the aid of a Gleeble 3500 thermomechanical simulator. Stress-strain curves, processing map, and constitutive equation were developed and the following conclusions were made:

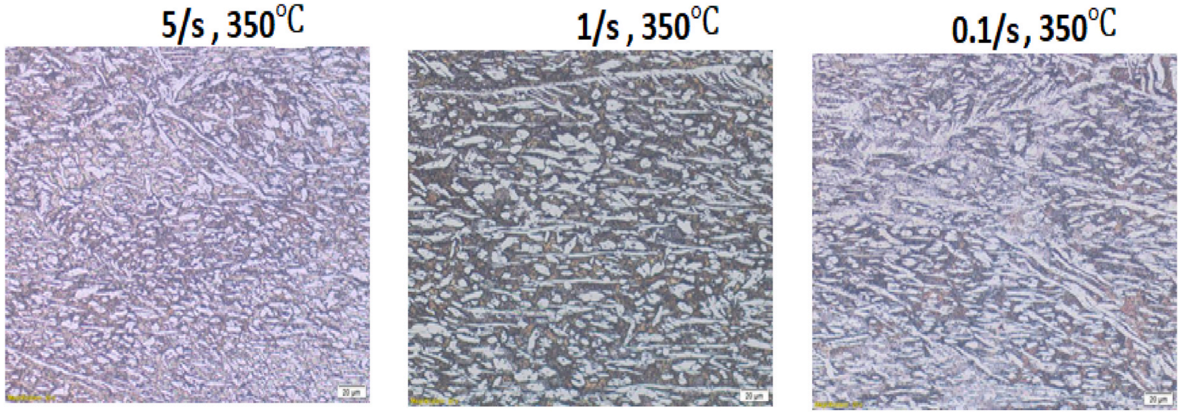

Fig. 7. Microstructures of Cu-Zn-Al-Ni SMA showing coarse dendritic structures at 350 $^{\circ}C$ and strain rate of 0.1, 1, and 5s^{-1}.

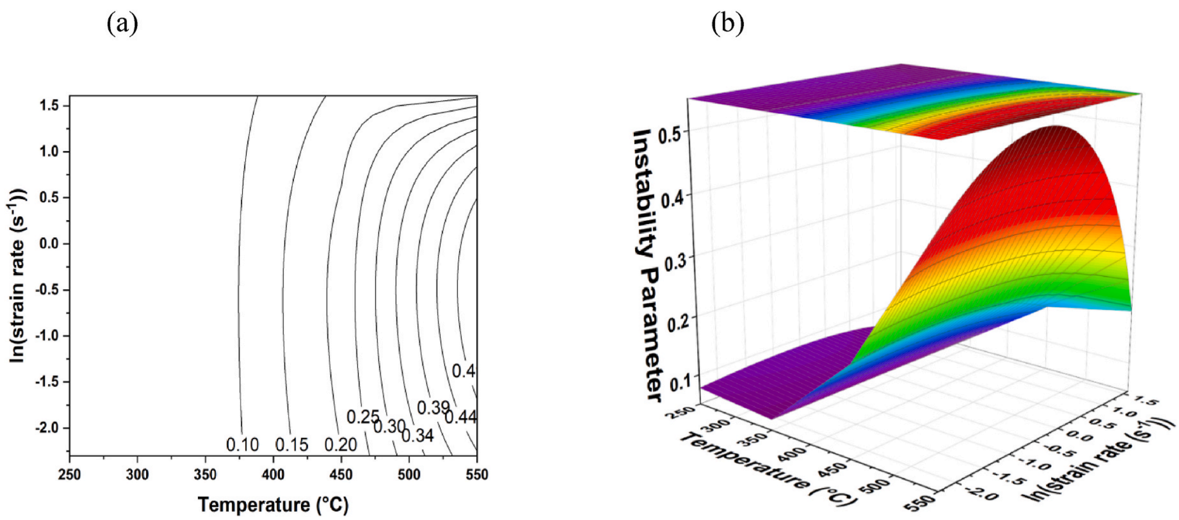

Fig. 8. Instability map of Cu-Zn-Al-Ni SMA: (a) 2D Instability contour line map (b) 3D Instability surface map.

i. The peak flow stress of Cu-Zn-Al-Ni SMA during hot compression is sensitive to the deformation temperature and the strain rate. The flow stress increases with the decrease of deformation temperature and the increase of strain rate.
ii. The constitutive equation of Cu-Zn-Al-Ni SMA is derived given that the flow stress is a function of the strain rate and temperature. The constitutive equation of the alloy can be expressed as:

$$\sigma = \frac{1}{0.0044}\ln\left\{\left(\frac{Z}{1.75034E14}\right)^{\frac{1}{4.54}} + \left[\left(\frac{Z}{1.75034E14}\right)^{\frac{2}{4.54}} + 1\right]^{\frac{1}{2}}\right\}$$

iii. The activation energy for the hot deformation of Cu-Zn-Al-Ni SMA was determined to be 154.34 kJ/mol which is about 24 % lower than the activation energy for self-diffusion of copper.
iv. The stress exponent value (n) is determined to be ≈ 4.54 which confirms the dominance of DRX over work hardening deformation mechanism as $n < 5$ and this is in agreement with the microstructures of the hot deformed samples.
v. The values for R2 and AARE for Cu-Zn-Al-Ni SMA were determined to be ≈ 0.93 and ≈ 0.68 respectively. The R2 values show a positive correlation between the two variables for all the deformed samples whereas a low AARE value signifies that the constitutive equation derived in this work was reliable in predicting the flow stress of Cu-Zn-Al-Ni SMA during the hot deformation process.
vi. Flow instability occurs at low temperatures ($250 - 350^{\circ}C$) and strain rates ranging from 0.1 to 5 s^{-1}, with characteristic shear bands, dendrite structures, and micro-cracks in their microstructure. Therefore, it is necessary to avoid processing the alloy in this region or under this condition.
vii. The optimal condition for hot deformation of the SMA is determined to be the temperature of 550 $^{\circ}C$ and strain rates of between 0.1 and 2.5s^{-1}. These conditions result in stable flow with microstructures consisting of uniform and fine equiaxed grains which is due to the occurrence of dynamic recrystallization.
viii. This work established that the stress exponent derived from the constitutive equation and the processing map developed using dynamic materials modeling are efficient in predicting the deformation mechanism and workability response of this alloy.

CRediT authorship contribution statement

Kenneth Kanayo Alaneme: Writing – review & editing, Validation, Supervision, Project administration, Methodology, Funding acquisition, Data curation, Conceptualization. **Sodiq Abiodun Kareem:** Writing – original draft, Methodology. **Justus Uchenna Anaele:** Writing – original draft, Methodology. **Michael Oluwatosin Bodunrin:** Supervision, Methodology, Investigation, Formal analysis.

Declaration of competing interest

I humbly write on behalf of my co-authors to submit our manuscript titled: Hot deformation behaviour, constitutive equations and processing map of Cu-Zn-Al-Ni shape memory alloy, for your consideration for publication in your highly esteemed journal.

The authors declare that there is no conflict of interest; Also, that:

i. The manuscript is not under consideration for publication elsewhere
ii. The authors are aware of the Editorial policy of the journal.

Acknowledgement

The authors wish to appreciate the support of their respective institutions, and the National Research Foundation (NRF), South Africa through the Grant No: 138062, administered by The University of Johannesburg, South Africa.

Data availability

Data will be made available on request.

References

[1] S. Zareie, A.S. Issa, R.J. Seethaler, A. Zabihollah, Recent advances in the applications of shape memory alloys in civil infrastructures: a review, in: Structures, vol. 27, Elsevier, 2020, October, pp. 1535–1550.
[2] K.K. Alaneme, E.A. Okotete, J.U. Anaele, Structural vibration mitigation–a concise review of the capabilities and applications of Cu and Fe based shape memory alloys in civil structures, J. Build. Eng. 22 (2019) 22–32.
[3] J.U. Anaele, K.K. Alaneme, J.A. Omotoyinbo, Wear and corrosion behavior of selected up-quenched and step-quenched CuZnSn shape memory alloys, Manuf. Rev. 10 (2023) 16.
[4] M. Gholami-Kermanshahi, Y.Y. Wu, G. Lange, S.H. Chang, Effect of alloying elements (Nb, Ag) on the damping performance of Cu–Al–Mn shape memory alloys, Journal of Alloys and Compd 930 (2023) 167438, https://doi.org/10.1016/j.jallcom.2022.167438.
[5] N.M. Dawood, A.A.R. Abid, Effect of aging on corrosion behavior of martensite phase in Cu-Al-Ni shape memory alloy, Key Eng. Mater. 911 (2022) 96–102, https://doi.org/10.4028/p-3jm065.
[6] İ. Özkul, O. Karaduman, T. Şimşek, T. Şimşek, C.A. Canbay, P.A. Ibrahim, I.A. Arpa, Experimental investigation of the effects of different quaternary elements (Ti, V, Nb, Ga, and Hf) on the thermal and magnetic properties of CuAlNi shape memory alloy, J. Mater. Res. 37 (14) (2022) 2271–2281.
[7] C. Shao, Y. Huang, Advances in shape memory alloy-based Reinforcement in steel structures: a review, Buildings 13 (11) (2023) 2760.
[8] E.M. Mazzer, M.R. da Silva, P. Gargarella, Revisiting Cu-based shape memory alloys: recent developments and new perspectives, J. Math. Res. 37 (1) (2022) 162–182, https://doi.org/10.1557/s43578-021-00444-7.
[9] S. Singh, S. Karthick, I.A. Palani, Design and development of Cu–Al–Ni shape memory alloy coated optical fiber sensor for temperature sensing applications, Vacuum 191 (2021) 110369.
[10] J. Tian, W. Zhu, Q. Wei, S. Wen, S. Li, B. Song, Y. Shi, Process optimization, microstructures and mechanical properties of a Cu-based shape memory alloy fabricated by selective laser melting, J. Alloys Compd. 785 (2019) 754–764.
[11] K.K. Alaneme, J.U. Anaele, E.A. Okotete, Martensite aging phenomena in Cu-based alloys: effects on structural transformation, mechanical and shape memory properties: a critical review, Scientific African 12 (2021) e00760.
[12] K.A. Abdelghafar, A.A. Hussein, E.M. Elbanna, M.A. Waly, M.M. Ibrahim, Influence of thermo-mechanical treatment on mechanical properties and shape memory effect of CuAlNiMnTi shape memory alloys, Intermetallics 136 (2021) 107251.
[13] H. Xu, Y. Zhao, K. Cheng, J. Zhong, N. Ding, L. Liu, L. Zhang, High-throughput determination of interdiffusivity matrices and atomic mobilities in Cu-rich fcc Cu-Sn-Zn alloys by using the experimental composition profiles and HitDIC, J. Alloys Compd. 944 (2023) 169205.
[14] K.K. Alaneme, J.U. Anaele, M.O. Bodunrin, Hot deformation processing of shape memory alloys: a review of effects on plastic flow behaviour, deformation mechanisms, and functional characteristics, Alex. Eng. J. 61 (12) (2022) 12759–12783.
[15] G.V.d.M. Candido, D.F. Oliveira, I.C.A. Brito, R.E. Caluête, B.H.d.S. Andrade, D.G. L. Cavalcante, Effect of hot rolling on the thermomechanical properties of a superelastic Cu-Al-Be-Cr alloy, Math. Res. 23 (1) (2020) e20190542, 10.1590/1980- 5373-mr-2019-0542.
[16] N. Nayan, G. Singh, S.V.S.N. Murty, P.R. Narayan, M. Mohan, P. V. Venkitakrishnan, U. Ramamurty, Effect of ternary additions of Cu and Fe on the hot deformation behavior of NiTi shape memory alloy - a study using processing maps, Intermetallics 131 (2021) 107084, https://doi.org/10.1016/j.intermet.2021.107084, 1-13.
[17] M. Morakabati, M. Aboutalebi, S. Kheirandish, A.K. Taheri, S.M. Abbasi, Hot tensile properties and microstructural evolution of as cast NiTi and NiTiCu shape memory alloys, J. Mater. Des. 32 (4) (2011) 406–413.
[18] K.K. Alaneme, M.O. Bodunrin, L.H. Chown, N.B. Maledi, Flow stress behaviour and microstructural analysis of hot deformed Aluminium matrix composites reinforced with CuZnAlNi shape memory alloy particles, Rev. Metal. (Madr.) 56 (2) (2020) e170.
[19] P. Yong, X. Zhu, J. Yanlin, Z. Rui, Y. Jiang, Q. Wenting, L. Zhou, Hot deformation behavior of a CuAlMn shape memory alloy, J. Alloys Compd. 845 (2020) 156161, https://doi.org/10.1016/j.jallcom.2020.156161, 1-16.
[20] M. Belbasi, M.T. Salehi, S.A.A.A. Mousavi, S.M. Ebrahimi, A study on the mechanical behavior and microstructure of NiTiHf shape memory alloy under hot deformation, Mater. Sci. Eng., A 560 (2013) 96–102.
[21] S.A. Kareem, J.U. Anaele, E.O. Aikulola, O.F. Olarewaju, B.O. Omiyale, M. O. Bodunrin, K.K. Alaneme, Hot deformation behaviour, constitutive model description, and processing map analysis of superalloys: an overview of nascent developments, J. Mater. Res. Technol. (2023), https://doi.org/10.1016/j.jmrt.2023.09.180.
[22] S. Santosh, R. Praveen, V. Sampath, Influence of cobalt on the hot deformation characteristics of an NiTi shape memory alloy, Trans. Indian Inst. Met. 72 (2019) 1465–1468.
[23] K.K. Alaneme, J.U. Anaele, S.A. Kareem, Hot deformability, microstructural evolution and processing map assessment of high entropy alloys: a systematic review, J. Mater. Res. Technol. 26 (2023) 1754–1784.
[24] S. Jiang, Y. Wang, B. Yan, Y. Zhang, Hot workability of FeMnSiCrNi shape memory alloy based on processing map and martensitic transformation, J. Alloys Compd. 806 (2019) 1153–1165.
[25] R.R. Eleti, T. Bhattacharjee, A. Shibata, N. Tsuji, Unique deformation behavior and microstructure evolution in high temperature processing of HfNbTaTiZr refractory high entropy alloy, Acta Mater. 171 (2019) 132e145.
[26] Y.Q. Zhang, S.Y. Jiang, Y.N. Zhao, S.W. Liu, Constitutive equation and processing map of equiatomic NiTi shape memory alloy under hot plastic deformation, Trans. Nonferrous Metals Soc. China 26 (8) (2016) 2152–2161.
[27] Y. Wang, S. Jiang, Y. Zhang, Processing map of NiTiNb shape memory alloy subjected to plastic deformation at high temperatures, Metals 7 (9) (2017) 328.
[28] C. Zener, J.H. Hollomon, Effect of strain rate upon plastic flow of steel, J. Appl. Phys. 15 (1) (1944) 22–32.
[29] Y. Sun, Q. Pan, Z. Huang, W. Wang, X. Wang, M. Li, J. Lai, Evolutions of diffusion activation energy and Zener–Hollomon parameter of ultra–high strength Al–Zn–Mg–Cu–Zr alloy during hot compression, Prog. Nat. Sci.: Mater. Int. 28 (5) (2018) 635–646.
[30] K.K. Alaneme, S.A. Kareem, M.O. Bodunrin, Hyperbolic–sine constitutive model determined hot deformation mechanisms and workability response of Al–Zn/Cu and Al–Zn/SiC based composites, Results in Engineering 19 (2023) 101255.
[31] K.K. Alaneme, S.A. Babalola, L.H. Chown, N.B. Maledi, M.O. Bodunrin, Study on hot deformation behavior and workability of stir–cast Al6063–6wt.% steelp based composites, J. Mech. Behav. Mater. 30 (1) (2021) 110–117.
[32] M.O. Bodunrin, Flow stress prediction using hyperbolic–sine Arrhenius constants optimised by simple generalised reduced gradient refinement, J. Mater. Res. Technol. 9 (2) (2020) 2376–2386.
[33] R.D. Janani, S.A. Salman, K.P. Priyadharshini, V. Karthik, Effect of composition on the stacking fault energy of copper-nickel alloys using molecular dynamics simulations, Mater. Today: Proc. 39 (2021) 1796–1800.
[34] Y.V.R.K. Prasad, K.P. Rao, Mechanisms of high temperature deformation in electrolytic copper in extended ranges of temperature and strain rate, Mater. Sci. Eng., A 374 (1–2) (2004) 335–341.
[35] X.M. Chen, M.T. Ning, H.W. Hu, Y.C. Lin, X.J. Zhou, J. Zhang, et al., Characterization of hot deformation behavior and optimization of hot workability for GH4698 superalloy, Mater. Char. 201 (2023) 112916, https://doi.org/10.1016/j.matchar.2023.112916.
[36] H. Cui, Y. Tan, R. Bai, L. Ning, X. You, C. Cui, et al., Deformation and recrystallization behavior of the new Ni-Co based superalloy ingot material prepared by electron beam smelting layered solidification, J. Alloys Compd. 934 (2023) 167880, https://doi.org/10.1016/j.jallcom.2022.167880.
[37] S. Guo, S. Wu, J. Guo, Y. Shen, W. Zhang, An investigation on the hot deformation behavior and processing maps of CoNi-Cr-W-based superalloy, J. Manuf. Process. 74 (2022) 100e11, https://doi.org/10.1016/j.jmapro.2021.11.060.
[38] S. Sampath, Influence of copper on the deformation behavior of NiTi shape memory alloys in isothermal compression, Mater. Today: Proc. 72 (2023) 2428–2431.
[39] Y.V.R.K. Prasad, H.L. Gegel, S.M. Doraivelu, J.C. Malas, J.T. Morgan, K.A. Lark, et al., Modeling of dynamic material behavior in hot deformation: forging of Ti-6242, Metallurgical Trsansactions A 15 (1984) 1883e92, https://doi.org/10.1007/BF02664902.
[40] W. Liu, Z. Liu, H. Zhang, J. Ruan, H. Haung, X. Zhou, et al., Hot deformation behavior and new grain size model of hot extruded FGH4096 superalloy during hot compression, J. Alloys Compd. 938 (2023) 168574, https://doi.org/10.1016/j.jallcom.2022.168574.
[41] Y. Zhu, Y. Cao, Q. He, J. Zhang, R. Luo, H. Di, et al., Threedimensional hot processing map of a nickel-based superalloy (Alloy 925) established by modified artificial neural network model, Intermetallics 141 (2022) 107433, https://doi.org/10.1016/j.intermet.2021.107433.